ACS APPLIED MATERIALS & INTERFACES

Research Article

www.acsami.org

Binding of Alkenes and Ionic Liquids to B–H-Functionalized Boron Nanoparticles: Creation of Particles with Controlled Dispersibility and Minimal Surface Oxidation

Jesus Paulo L. Perez,[†] Jiang Yu,[†] Anna J. Sheppard,[‡] Steven D. Chambreau,[§] Ghanshyam L. Vaghjiani,[‡] and Scott L. Anderson*,[†]

[†]Department of Chemistry, University of Utah, 315 South 1400 East, Salt Lake City, Utah 84112, United States

[§]ERC, Inc., and [‡]Propellants Branch, Aerospace Systems Directorate, Air Force Research Laboratory, AFRL/RQRP, Edwards Air Force Base, California 93524, United States

ABSTRACT: The interaction of B–H-functionalized boron nanoparticles with alkenes and nitrogen-rich ionic liquids (ILs) is investigated by a combination of X-ray photoelectron spectroscopy, FTIR spectroscopy, dynamic light scattering, thermogravimetric analysis, and helium ion microscopy. Surface B–H bonds are shown to react with terminal alkenes to produce alkyl-functionalized boron particles. The interaction of nitrogen-rich ILs with the particles appears, instead, to be dominated by boron–nitrogen bonding, even for an ILs with terminal alkene functionality. This chemistry provides a convenient approach to producing and capping boron nanoparticles with a protective organic layer, which is shown to protect the particles from oxidation during air exposure. By controlling the capping group, particles with high dispersibility in nonpolar or polar liquids can be produced. For the particles capped with ILs, the effect of particle loading on hypergolic ignition of the ILs is reported.

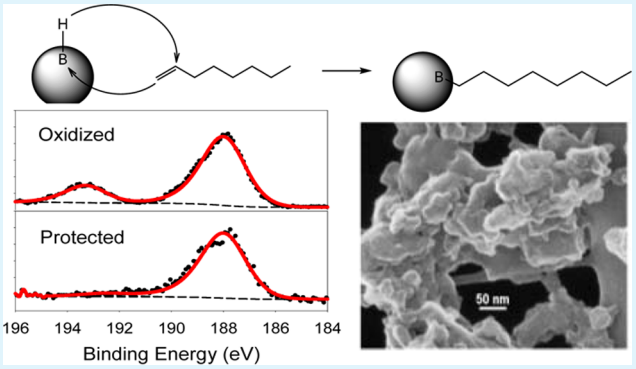

KEYWORDS: *energetic materials, ionic liquids, alkylation, boron, nanoparticles*

INTRODUCTION

The fact that boron's volumetric heat of combustion (137.8 kJ/mL)[1] is significantly higher than those for typical liquid fuels (35–38 kJ/mL), and of those of combustible metals such as aluminum (83.8 kJ/mL) or magnesium (43.0 kJ/mL), makes it interesting as a fuel additive.[2−9] Several problems have inhibited use of boron for this purpose. Boron is refractory, thus combustion is inherently a heterogeneous process, limited by diffusion to and from the surface. Increasing particle dispersion by reducing the size can potentially mitigate this problem; however, because unprotected boron is passivated with an oxide layer, reduction in size is accompanied by an increase in the mass fraction of incombustible oxide. The oxide layer also inhibits ignition, and thus production of particles that are air stable, but unoxidized, could potentially improve ignition and allow use of smaller particles, with higher surface area per gram.

Ignition and combustion rates are not the only challenge for boron combustion. In particular, when H is present, there is a tendency toward partial combustion, forming HOBO(gas), rather than the most thermodynamically favorable B_2O_3(liq.) product. Use of unoxidized nanoparticles does not directly address this issue. However, because incomplete combustion is a kinetics problem, it is possible that faster ignition and combustion might improve the B_2O_3 branching ratio, or allow condensation of HOBO to oligomers, either of which significantly increase the heat release.

Here we describe production of boron nanoparticles, capped with various protecting organic layers, that are air stable with insignificant oxide formation. The capping layers also allow control over the dispersibility of the particles in different media. For example, alkyl surface functionalization makes the particles highly dispersible in hydrocarbon fuels, whereas ionic liquid capping makes the particles dispersible in ionic liquids, including propellants.

The capping process shown here takes advantage of the discovery that milling boron powder in H_2 results in efficient production of hydrogen-terminated boron nanoparticles.[10] Particles with up to 5 wt % (36 mol %) hydrogen loading were produced, and detailed theory showed that it is energetically favorable to saturate the boron surface with H, mostly in the form of terminal B–H bonds, and that interstitial H sites are energetically unfavorable. In that case, the high hydrogen loading implies H-capped surface areas near 1200

Received: March 18, 2015
Accepted: April 24, 2015
Published: April 24, 2015

DOI: 10.1021/acsami.5b02366
ACS Appl. Mater. Interfaces 2015, 7, 9991−10003

m^2/g, consistent with the observation of thin, platelike particle structures by scanning transmission electron microscopy (STEM[10]) and helium ion microscopy (HeIM - see below). The presence of terminal B−H bonds was confirmed by FTIR analysis, giving rise to a strong feature at 2507 cm^{-1}, similar to the frequencies observed for B−H bonds in boranes (2475−2730 cm^{-1}).[11]

Here, we exploit the B−H surface termination of the H_2-milled particles to couple alkenes to the surfaces, generating unoxidized, alkyl-protected surfaces. The process is reminiscent of hydroboration chemistry, commonly used to convert alkenes to alcohols. The first step in hydroboration is to react a borane with an alkene, such that B−H adds across the double bond, making C−H and C−B bond, and producing an alkylborane.[12−15] The alcohol is then generated by reacting the alkylborane with an oxidizing agent. The hope was that H-terminated boron particles would have borane-like reactivity with alkenes, producing alkyl-functionalized particles as shown in Scheme 1 for the case of 1-octene. For boron particles

Scheme 1. Proposed Reaction of Hydrogenated Boron Nanoparticles with Octene

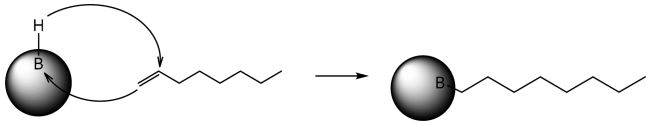

saturated with B−H bonds, the alkyl density might then be high enough to protect the particles from oxidation under ambient conditions.

We demonstrate that this approach can be used to generate boron nanoparticles robustly capped with alkyl chains of variable length, such that the resulting particles are oxide free even after air drying at elevated temperatures, and are soluble in hydrocarbons. We also examine binding of several ionic liquid (IL) capping agents, including one (1-allyl-3-methylimidizolium dicyanamide, [AMIM][DCA]) that has a double bond. For the IL-capped particles, hypergolic ignition as a function of boron loading in the IL is also studied. It should be noted that this approach is complementary to the use of IL propellants where boron is incorporated into the IL constituents directly, as recently reviewed by Zhang and Shreeve.[16]

This work follows on earlier studies that demonstrated efficient production of boron nanoparticles in the 50−150 nm size range by ball milling, with simultaneous capping by ligands including oleic acid[17,18] and several hypergolic ionic liquids (ILs), including 1-methyl-4-amino-1,2,4-triazolium dicyanamide ([MAT][DCA]) and 1-butyl-3-methylimidizolium dicyanamide ([BMIM][DCA]).[19,20] In each case, the particles were air-stable with minimal oxidation, and highly dispersible in hydrocarbons (oleic acid-capped) or ILs propellants (IL-capped). In these previous examples, capped particles were prepared by simply milling boron feedstock together with oleic acid or ILs, such that the capping agents were present to bind to the boron surfaces exposed by fracturing. Such "one-pot, one step" methods are simple, but may be unsuitable for some applications.

One such application is use of boron nanoparticles for boron neutron capture therapy, where the particles need to be biocompatible (i.e., water-soluble). The ideal ligand would have a polar group that binds to boron, leaving additional polar groups extending into the solvent to confer water solubility. The problem is that boron has high affinity for O, N, halogens, etc., and thus tends to react with all the polar moieties under milling conditions. One approach to increasing ligand diversity is to first produce boron particles capped with a ligand that is compatible with milling, and then use ligand exchange to change the surface functionalization. Zharov et al.[21] used this approach to replace the initial oleic acid capping layer with dopamine, to generate water-soluble boron nanoparticles, albeit with substantial surface oxidation. The capping approach proposed here is somewhat different, because we react a ligand with a functionalized surface, rather than displacing an existing ligand, and are able to add the capping agent without significant surface oxidation.

EXPERIMENTAL METHODOLOGY

Milling was done using a planetary mill (Retsch PM400) at 300 rpm for a total of 16 h. Micron-sized boron powder (97%, ~2 μm particles) from C.R. Supply Co. (West Hills, CA) was milled with H_2 gas (industrial grade, Airgas USA, LLC, Denver, CO) to produce boron nanoparticles with their surfaces terminated by B−H bonds, as discussed elsewhere.[10] Briefly, 2 g of boron feedstock was placed inside a 250 mL tungsten carbide-lined milling jar with 160 g of tungsten carbide milling balls. The jar was sealed and purged with Ar three times by alternatively evacuating and filling the jar via a valve attached to the modified jar lid.[22] The jar was then pressurized with H_2 gas to 4 atm absolute pressure. The milling program alternated 30 min milling periods with 5 min rest/cooling periods, reversing direction in each milling period. Gas pressure inside the jar was measured after the milling process to monitor uptake of H_2 by the boron. As noted above, this procedure was shown to generate boron particles with high surface area, terminated by B−H bonds.

To cap the particles with the alkene or ionic liquid of interest, we opened the jar in an N_2 glovebox and added 5 mL of the ligand. The jar was then resealed, Ar purged, filled with an overpressure of Ar, and then milled at 100 rpm for another 12 h to thoroughly mix the boron and the liquid capping agent. The "mix milling" was used to break up weakly bound aggregates, and to ensure that the agent thoroughly coated the particles, but low speed was used to minimize fracturing of primary boron particles, which would expose fresh, non-hydrogenated boron surfaces. Mixing was done under argon, rather than H_2, in order to avoid possible hydrogenation of the unsaturated ligands under milling conditions. The result of the mixing process was a viscous mixture of particles in excess ligand. To extract the particles, 150 mL of an appropriate solvent was added to the jar, and the mixture was milled under argon for an additional 6 h at 100 rpm to thoroughly disperse the nanoparticles in the solvent. Hexane was used as the solvent for the particles milled with alkenes, and acetone was used for the IL-coated particles. Octene, octadecene, and [AMIM][DCA] were obtained from Aldrich, with stated purities of 98.5, 95, and 98.5%, respectively. [MAT][DCA] was synthesized at the Air Force Research Laboratories using procedures described previously,[23] with estimated purity of 98%. Liquids were degassed by freeze−pump−thaw cycles, N_2 sparging, or prolonged pumping (for the ILs), before use.

The nanoparticles produced by mix milling with octene/octadecene and with ILs were found to be highly dispersible in hexane and in acetone, respectively, as expected for particles capped with alkyl or ionic/polar ligands. To remove excess capping agent to allow spectroscopic characterization of the particle surfaces, we repeatedly solvent washed the particles. The particles prepared with alkenes were precipitated from hexane suspensions by addition of ethanol, in which the alkenes themselves are moderately soluble, and then washed in excess ethanol. The IL-capped particles were centrifuged out of acetone suspensions and redispersed in fresh acetone, and the dispersion/centrifugation process was repeated three times with fresh acetone, in which the ILs are highly soluble. Finally, the particles were oven-dried at a pressure of a few Torr (of air) to remove any volatiles. Size distributions of the as-milled boron nanoparticles determined by scanning electron microscopy (SEM) and dynamic

DOI: 10.1021/acsami.5b02366
ACS Appl. Mater. Interfaces 2015, 7, 9991−10003

light scattering (DLS) were reported in a paper describing the IL-milling process.[19] SEM contrast for boron is relatively poor, and here we report imaging of the [AMIM][DCA]-capped particles using helium ion microscopy (Zeiss Orion).

To probe binding of ligands to the particle surfaces, we analyzed samples by attenuated total reflectance Fourier transform infrared spectroscopy (ATR-FTIR) (Nicolet iS10, Thermo Fisher Scientific). Samples, washed and dried as described above, were pressed directly onto the instrument's diamond ATR crystal, and IR spectra were obtained with resolution of 1 cm^{-1} in 15 independent scans, and then averaged. To study surface oxidation of the particles, they were analyzed by X-ray photoelectron spectroscopy (XPS) (Kratos, Axis Ultra). Ligand-capped particles were repeatedly washed as described above, and then dried overnight in an oven. The alkene-capped particles were heated at low vacuum (~10 mTorr, 350 K) to ensure that any volatile residue was eliminated. IL-capped particles were simply heated at atmospheric pressure to 325 K. All particles were transported in air, and loaded into the XPS instrument's vacuum system using carbon tape to hold a thin layer of particles to the sample bar. Removing volatiles is important, not only to protect the ultrahigh vacuum in the XPS instrument, but also to minimize attenuation of signal from the boron by organic adsorbates. XPS analysis was also done on uncapped, H_2-milled boron particles, which are highly reactive with oxygen. Those particles were first passivated by exposure to a few Torr of air in the glovebox load lock chamber, leading to formation of a stabilizing oxide layer, and then pressed onto carbon tape attached to the XPS sample bar.

Hypergolic ignition experiments were performed using rapid scan Fourier transform infrared (RS-FTIR) absorption spectroscopy as described elsewhere,[24] with spectra typically acquired every 10 ms over the 3850–590 cm^{-1} range, with 4 cm^{-1} spectral resolution. The infrared beam was focused above the reaction zone by means of gold-coated parabolic mirrors through KRS-5 windows. The reaction vessel, consisting of a glass cuvette, was contained within a stainless steel chamber under constant nitrogen purge. Small samples (~0.1 mL) of ionic liquids with and without boron nanoparticles were placed in the cuvette in the stainless steel chamber and the oxidizer (white fuming nitric acid (WFNA)) was dropped onto the samples via a gastight syringe through a septum at the top of the chamber. As the oxidizer dropped onto the sample, it interrupted a HeNe laser beam, and the drop in signal at a photodiode was used to trigger the FTIR spectrometer.

The concentration of boron nanoparticles in the hypergolic ILs was varied in order to determine the dependence of ignition delay time on the concentration of nanoparticles. Samples prepared with IL capping (without solvent washing) were approximately 25 wt % boron in the IL, and those samples were further diluted with the neat ILs to produce concentrations of roughly 12 and 6 wt %. The dilutions were made by mixing the appropriate weights of 25 wt % B-in IL samples with neat ILs on a shaker table for ~1 min until samples appeared homogeneous. Samples were remixed on the shaker table prior to any testing to ensure uniform dispersion of nanoparticles. Mixing was not performed in an inert atmosphere, but no signs of oxidation were observed.

Ignition delay times were evaluated using the RS-FTIR spectra. Known ignition products of the hypergolic ILs are CO_2, N_2O, and HNCO, and ignition onset was determined by the presence of CO_2. Most samples did not produce any visible light emissions when the HNO_3 made contact with the ionic liquids, but smoke was frequently seen and evidenced in the spectra via a baseline shift, usually accompanied by the known combustion products. The ignition delay time reported below should be considered as relative ignition delay time with respect to nanoparticle concentrations, as opposed to an absolute ignition delay time. Aspects of the experimental setup, notably the distance the oxidizer drop must fall before it first makes contact with the ionic liquid (~1 cm, which takes ~45 ms), and the distance the evolved products must travel before they first intercept the IR beam (~1 cm, time dependent on relative concentrations, temperature, etc.), make accurate ignition delays problematic. The uncertainty estimate for the ignition delay times is ±0.3 s.

Safe Handling. Unpassivated boron nanoparticles are pyrophoric, and ignite spontaneously upon contact with air. Until a particular batch of particles has been shown to be air stable, testing should be confined to small samples, and done well away from combustible materials. Drying of solvent-wetted particles may result in ignition after significant delays.

RESULTS AND DISCUSSION

Particle Size and Morphology. As noted in the introduction, the hydrogen loading of boron nanoparticles produced by milling in H_2 is quite high (5 wt %), and high level theory indicates that the only stable binding sites for hydrogen are on the surface of the boron, mostly in the form of terminal B–H bonds.[10] H or H_2 binding in interstitial or other sites within the boron bulk is found to be highly unfavorable energetically. If the high hydrogen loading is assumed to represent surface B–H bonds, then the hydrogen-accessible surface area would need to be ~1200 m^2/gram boron.

Figure 1 shows a helium ion micrograph of H_2-milled boron particles, which were rendered air stable by mix-milling with

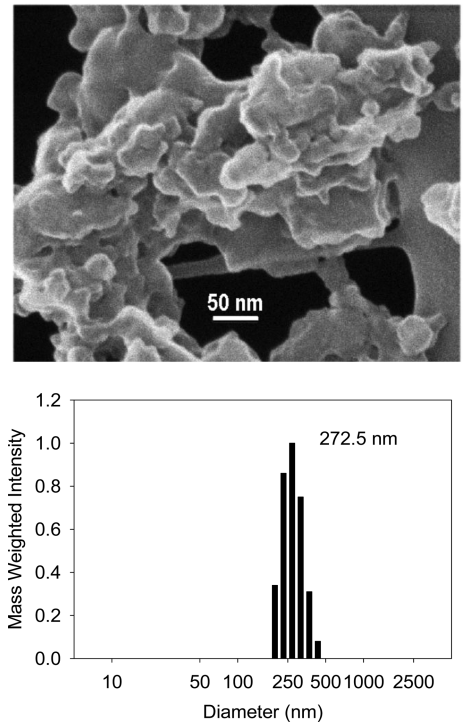

Figure 1. Top: Helium ion micrograph of H_2-milled boron nanoparticles capped with [AMIM][DCA]. Bottom: DLS of the same particles in acetone suspension.

[AMIM][DCA], then deposited onto a lacey carbon TEM grid by solvent casting. As the image shows, the primary particles appear to have flat, plate-like structures, consistent with previously reported SEM and STEM images for H_2-milled boron, which were, however, much less distinct.[10] The similarity suggests that the low-speed mix milling used in the capping process does not strongly alter the particle size or morphology. The primary particles have lateral dimensions ranging from ~10 nm to several hundred nanometers, but the flattened, convoluted structures would have high surface areas, consistent with the large hydrogen uptake observed in the milling process. In addition, the particles appear to be aggregated. Some of this aggregation almost certainly occurred

DOI: 10.1021/acsami.5b02366
ACS Appl. Mater. Interfaces 2015, 7, 9991–10003

by cold welding during particle production by dry milling in H_2, but there may have additional aggregation during drying of the solvent-cast particle suspension. DLS analysis of these particles in acetone suspension show additional aggregation, resulting in a volume-weighted size distribution extending between ~170 and 470 nm, with average size near 270 nm.

Given that the reaction of H_2 with boron to form B−H-terminated surfaces is calculated to be exothermic and spontaneous under milling conditions, a likely explanation for the high hydrogen loading is that hydrogen efficiently saturates surfaces as they form during milling, including surfaces of cracks and internal surfaces between primarily particles in aggregates, which may form by cold-welding of primary particles during milling. Such surfaces may or may not be accessible to capping agents during subsequent mix milling. This issue is discussed further below.

Alkyl-Capped Boron Nanoparticles. Binding of 1-octene to the boron particles was examined by IR spectroscopy, as shown in Figure 2. The top spectrum is for H_2-milled boron

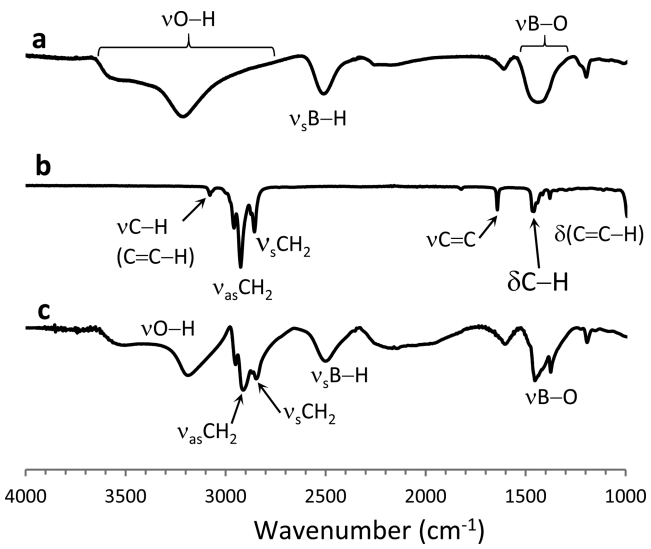

Figure 2. FTIR spectra of (a) H_2-milled boron nanoparticles, (b) neat 1-octene, and (c) H-milled boron nanoparticles that were mix-milled with 1-octene.

particles, without any organic capping ligands. There is a strong peak at 2507 cm^{-1} assigned to stretching of terminal B−H bonds, based on its similarity to B−H stretch frequencies (2475−2730 cm^{-1}) observed for boranes.[11] Note the presence of strong bands in the 3400−3000 cm^{-1} range, near 1350 cm^{-1}, and at 1197 cm^{-1}, assigned to O−H stretching, B−O stretching, and B−O−H out-of-plane bending modes, respectively.[10] These bands arise because the sample was exposed to air in the process of obtaining the IR spectrum, leading to oxidation, as also shown by XPS, below. Evidently, B−H termination does not passivate the surface against oxidation, which is not surprising given the air-sensitivity of many boranes.

The middle spectrum in Figure 2 is for neat 1-octene, with sharp bands observed at 3078, 2958, 2856, and 1641 cm^{-1} corresponding to the stretch of the alkenyl (C═C−H) C−H bonds, the asymmetric and symmetric C−H stretches of the alkyl (CH_2) groups, and the C═C stretch vibrations, respectively.[25] C−H bending modes were also observed for alkyl (1460 cm^{-1}) and alkenyl (906 cm^{-1}) groups. The final spectrum is for a sample prepared by milling boron in H_2, then mix milling with 1-octene, followed by washing to remove excess octene, and oven drying. It can be seen that modes associated symmetric and asymmetric CH_2 stretching modes are still present with high intensity, indicating that the surfaces have alkyl groups present that are stable with respect to repeated washing and oven drying. On the other hand, modes associated with the C═C bond, including the C═C stretch (1641 cm^{-1}) and the alkenyl C−H stretch (3078 cm^{-1}), are no longer observed, as would be expected if the C═C bond in octene had reacted with the B−H-functionalized surface.

Note also that the B−H stretch band (2507 cm^{-1}) is still present with substantial intensity after reaction with octene, indicating that reaction with octene does not completely consume all surface B−H groups. This is not surprising for several reasons. The average B−B spacing on the surface of amorphous boron can be estimated from the density to be ~0.19 nm, whereas the spacing between packed alkyl chains is expected to be in the 0.35−0.43 nm range.[26] As a result, steric considerations suggest that only roughly one-quarter of the surface B−H sites can be alkylated. Furthermore, while the hydrogen loading suggests that primary boron particles produced by H_2 milling are quite small, DLS and microscopy indicate that there is significant formation of aggregates, probably including aggregates that are cold-welded during the process of particle production by dry milling in H_2. Such aggregates are likely to contain B−H groups on internal surfaces of cracks or voids that remain unreacted because they are inaccessible to octene.

The spectrum also shows significant intensity for OH and BO stretches, suggesting that the surface is not completely passivated against oxidation during the oven drying and air exposure accompanying sample preparation for IR spectroscopy. The extent of oxidation in such samples is difficult to quantify by IR, because the samples undoubtedly have adventitious molecules adsorbed on their surfaces, some of which may be oxygen-containing. There may also have been some ethanol binding to the surfaces from the ultrasonic washing process used to remove excess octene.

The extent of oxidation of the particle surfaces can be probed more directly by XPS, as shown in Figure 3. The spectra shown have been scaled so that the main peak at 188 eV has constant intensity. The baselines shown were calculated using the Shirley algorithm to estimate the inelastic scattering contribution to the signal at each energy.[27] The alkene- and IL-capped samples were repeatedly ultrasonically washed in ethanol and acetone, respectively, to remove any capping molecules not strongly bound to the boron surfaces, and then oven-dried. All samples were exposed to air during the transfer to the XPS instrument.

The top spectrum is for an H_2-milled sample that was simply passivated by slow air exposure, and then transferred to the XPS instrument. The B 1s region shows a strong peak at 188 eV, due to elemental boron (B^0), as well as a substantial peak at 193 eV, which is assigned to oxidized boron (B^{3+}).[28] The effective attenuation length (EAL) for boron photoelectrons in boron oxide is 3 nm,[20] thus the XPS intensities are an exponentially weighted average of signals from the top ~6 nm of the sample. The spectrum, therefore, is interpreted as showing B^{3+} signal from a B_2O_3 layer on the surface of the particles, with B^0 signal from the unoxidized core of the particles, attenuated by passage through the oxide layer. The observation that hydrogen termination did not protect the particles from oxidation is unsurprising, given the reactivity of

DOI: 10.1021/acsami.5b02366
ACS Appl. Mater. Interfaces 2015, 7, 9991−10003

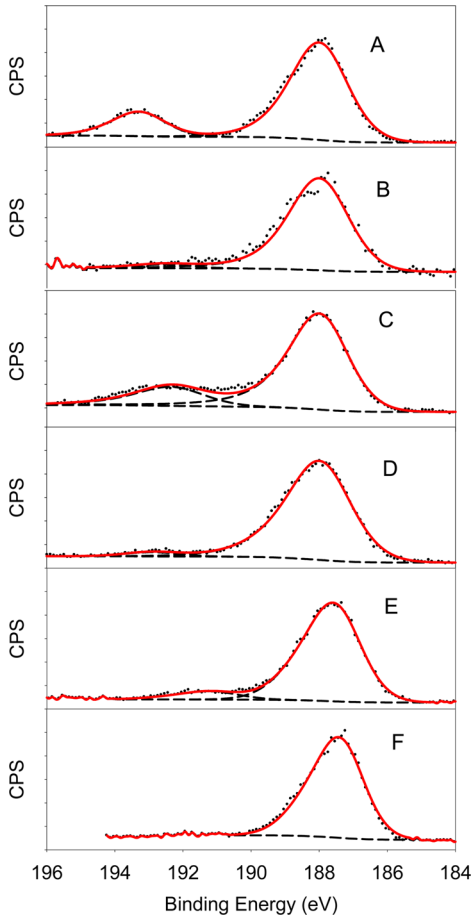

Figure 3. B 1s region XPS of (A) H_2-milled boron, (B) H_2-milled boron, mix- milled with 1-octene, (C) Ar-milled boron milled, mix-milled with 1-octene, (D) H_2-milled boron, mix-milled with 1-octadecene, (E) H_2-milled boron, mix-milled with [AMIM][DCA], and (F) H_2-milled boron, mix-milled with [MAT][DCA].

boranes, and the fact that hydrogen termination also does not passivate a number of metals.[29,30] In fact, the B^{3+}/B^0 ratio for these particles is substantially larger than the analogous ratio for a flat, air-exposed boron surface,[17] where the oxide layer thickness was estimated to be ~0.5 nm. The fact that the XPS-detectable oxide concentration is high in the nanoparticle sample is attributed (see below) to the particles having platelike morphology with high surface/volume ratio, and with many asperities, edges, and other substructures that increase the surface area, and which may be thin enough to oxidize completely through. In any case, the high B^{3+}/B^0 ratio is consistent with the conclusion that the air-accessible surface area of the particles is high.

For the sample milled in H_2 and then mix-milled with octene (spectrum B), there is almost no signal for B^{3+} at 193 eV, and little signal in the >190 eV range expected for partially oxidized boron, indicating that this sample was efficiently protected against air oxidation, presumably by binding of an octyl capping layer that is resistant to repeated ultrasonic solvent washing. The presence of the capping layer is also reflected by a ~30% reduction in the B^0 peak intensity, compared to that seen in the top spectrum, resulting from scattering of boron photoelectrons by the organic layer.

To verify that the protection against oxidation was really due to reaction of octene with the B−H-functionalized surface, boron was milled in argon, rather than H_2, and the resulting particles were mix-milled with octene, ultrasonically washed with ethanol, and oven-dried, using the same procedure used for spectrum B. As shown by spectrum C, this sample shows a large peak for oxidized boron, despite the observation that the particle size for Ar-milled boron is larger than that for H_2-milled boron.[10] The oxide peak is broadened and shifted to lower binding energy, suggesting formation of a distribution of B^{n+} oxidation states, but clearly boron is not well protected by simply mix milling octene with particles not having B−H surface functionality.

Spectrum D is for particles produced by milling in H_2, mix-milled with 1-octadecene, and then ethanol washed and dried as for the other samples. This sample does show an oxide peak at 193 eV, which is much smaller than those in spectra A and C, but still clearly larger than that for the H_2-milled boron protected by octene (spectrum B). This observation suggests, somewhat counterintuitively, that the 18 carbon alkene is less effective than octene in protecting the surfaces from oxidation. The less complete protection may simply reflect the higher viscosity and larger molecular size of octadecene, which may result in lower binding density due to steric effects, and less complete penetration into cracks or voids in aggregates, such that the B−H-functionalized surfaces are attacked by O_2 during subsequent washing and drying. Nonetheless, the extent of oxidation is still quite small compared to that in unprotected H_2-milled boron (spectrum A), or for Ar-milled boron mixed with octene (spectrum C).

Note that C 1s XPS signal was observed for all samples; however, this is not diagnostic for the presence of octene/octyl on the surface, because the particles were also exposed to ethanol and to adventitious carbonaceous molecules in the lab atmosphere. Spectral results for the IL-capped particles will be discussed below.

Another way of probing functionalization of the boron surfaces with alkenes is to compare the particle dispersibility in hexane. Samples for these experiments were washed ultrasonically in ethanol to remove weakly adsorbed alkenes, then dried and resuspended in hexane. The H_2-milled, octene-capped nanoparticles formed suspensions in hexane that were stable for the observation time (a few hours), as might be expected if the surfaces are functionalized with octyl groups conferring hydrocarbon solubility. Particles produced by Ar-milling, then mix-milled with octene, are substantially less dispersible in hexanes, with suspensions precipitating completely in less than 15 min. For reference, as-prepared H_2-milled boron, never exposed to octene, aggregates and settles out within seconds if dispersed in hexane. The IR, XPS, and dispersibility results all suggest that although there may be some binding of octene to unfunctionalized boron during milling, reaction with B−H surface groups is required to form a dense, stable capping layer, which both renders the particles hexane-compatible and minimizes air oxidation of dried powders.

Interaction of Hydrogenated Boron Particles with [MAT][DCA] and [AMIM][DCA]. We previously demonstrated that boron nanoparticles could be produced by milling boron powder in neat ionic liquids (ILs), including 1-methyl-4-amino-1,2,4-triazolium dicyanamide ([MAT][DCA]) and 1-butyl-3-methylimidizolium dicyanamide ([BMIM][DCA]).[19,20] The particles were shown to be air-stable and unoxidized; however, the milling process was inefficient because the ILs are quite viscous, becoming pastelike when heavily loaded with particles for milling. It was not judged prudent to mill in large

DOI: 10.1021/acsami.5b02366
ACS Appl. Mater. Interfaces 2015, 7, 9991−10003

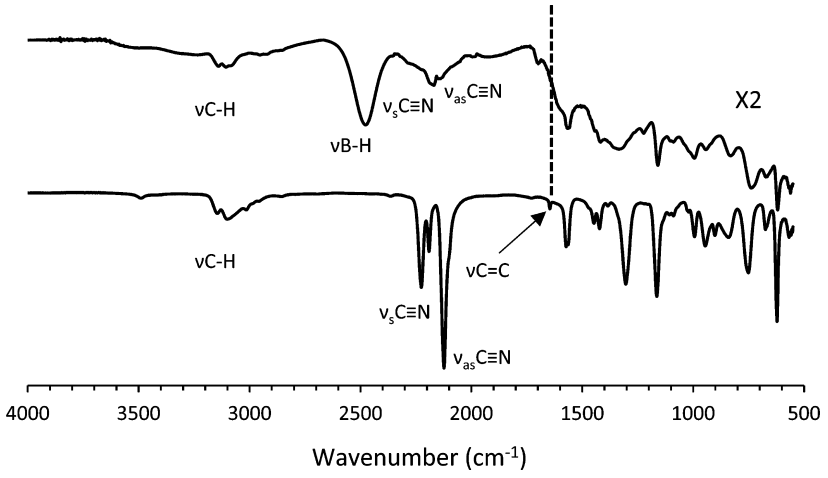

Figure 4. ATR-FTIR spectra of (top) H_2-milled boron capped with [AMIM][DCA] and (bottom) neat [AMIM][DCA].

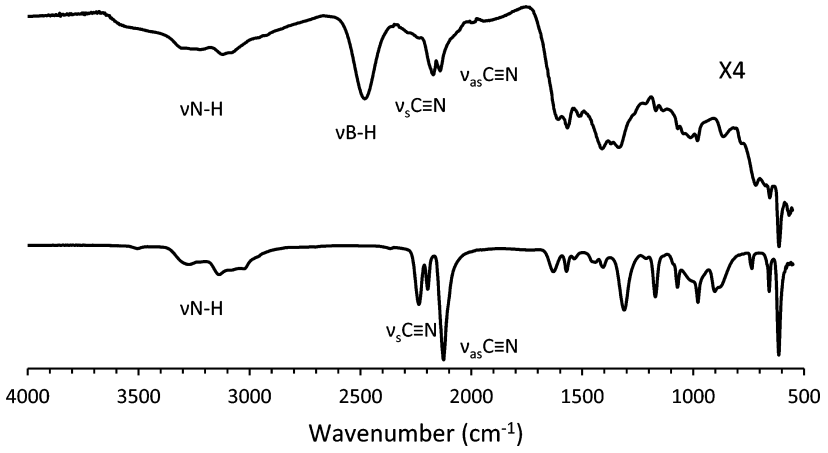

Figure 5. ATR-FTIR spectra of (top) H_2-milled boron capped with [MAT][DCA] and (bottom) neat [MAT][DCA].

excesses of the ILs, both because they are expensive, and because they could potentially decompose under milling condition, creating an explosion risk. We attempted to mitigate the viscosity problem by adding acetonitrile as a thinning agent; however, the resulting particles were not well passivated by the IL, and oxidized extensively upon air exposure. A two-step process was also tried, where milling in acetonitrile was used to make nanoparticles, which were subsequently capped with both [MAT][DCA] and [BMIM][DCA]. XPS analysis showed that the resulting particles were only partially passivated, showing significant oxidation upon air exposure.

The fact that dry-milling boron in H_2 leads to efficient nanoparticle production suggested the possibility of a two-step process to generate IL-capped nanoparticles, where H_2-milling is first used to generate nanoparticles, and then low speed mix-milling is used to coat the particles with ILs. We tested this approach with two ILs. [AMIM][DCA] has a C═C bond in its allyl group, and thus might potentially bind to B−H terminated boron particles via the same mechanism responsible for binding octene and octadecene. In addition, however, [AMIM][DCA] has N atoms on both the [AMIM] and [DCA] moieties that might be expected to complex with boron. [MAT][DCA] lacks the C═C functionality, but does have an amine group on the [MAT] moiety that could interact with boron.

From the fuels perspective, an important question is whether IL interaction with hydrogenated boron nanoparticles produces particles that are air-stable, and passivated against oxide formation during air exposure, and readily dispersible in polar media, such as the ILs themselves. Samples prepared as discussed above were stripped of excess ILs by repeated ultrasonic washing with acetone, in which both ILs are highly soluble. It is found that the [MAT][DCA]-capped boron particles form suspensions in acetone that are stable for ∼3 h, while acetone suspensions of [AMIM][DCA]-capped particles are stable for many hours, and uncapped H_2-milled boron precipitates from acetone suspension within a minute. The washed samples were drop cast onto copper foil, and air-dried overnight, before loading into the XPS instrument. B 1s XPS region scans are shown as spectra E and F in Figure 3. The spectrum for the [AMIM][DCA]-coated particles has essentially no signal at 193 eV (B^{3+}), however, there is a weak feature at 191.3 eV, suggesting formation of boron in some intermediate oxidation state. This 191.3 eV feature could result from a small extent of oxidation during air exposure, but it is also possible that it actually reflects boron binding to the [AMIM][DCA] ligands. We note that the B 1s binding energy for boron in BN is reported to be in the 190−191 eV range,[31] thus the peak might be taken as evidence for B−N bond formation. In either case, it is clear that interaction of hydrogenated boron with [AMIM][DCA] largely protected the particles from air oxidation. It is interesting that the sample prepared by interacting the hydrogenated boron particles with

DOI: 10.1021/acsami.5b02366
ACS Appl. Mater. Interfaces 2015, 7, 9991−10003

[MAT][DCA], which has no C=C bond to interact with the surface B−H functionality, shows even less evidence of boron oxidation. There is weak intensity around 192 eV, which again could result from formation of B−N bonds or from a small degree of air oxidation. It is not clear whether the weaker signal in the 191−192 eV range for [MAT][DCA], compared to [AMIM][DCA] reflects better protection against air oxidation, less formation of B−N bonds or some combination of the two factors. One might expect that the amine functionality of [MAT][DCA] might result in additional nitrogen bonding to the boron surface; however, the IR and zeta potential measurements discussed below suggest that for hydrogenated boron surfaces, interaction with the [DCA] anion dominates the bonding for both ILs.

To probe the nature of the IL-boron interaction, we took IR spectra, as shown in Figures 4 and 5 for particles milled in H_2, then capped with [AMIM][DCA] and [MAT][DCA], respectively. These samples were prepared by milling in H_2, mix-milling with the IL of interest, and then repeated ultrasonic washing in acetone, to remove any ILs not bound to the surfaces. The IR frequencies for the $[DCA]^-$ anion in $[NH_4][DCA]^-$ have been reported previously.[32,33] To help assign other features in the spectra, harmonic frequencies for both $[AMIM]^+$ and $[DCA]^-$ were calculated using GAUSSIAN09,[34] with the B3LYP and MP2 methods, and basis sets ranging up to 6-311++G**. The frequencies were found to be insensitive to basis set, and the B3LYP and MP2 frequencies were also quite similar. For simplicity, we quote frequencies from a B3LYP/6-31G** calculation, using the scale factor reported by Scott and Radom (0.9614) to convert the calculated harmonic frequencies to fundamental excitation frequencies.[35] Of course, the frequencies of some of the modes will be quite different in the IL, compared to the isolated cation and anion, and also differ somewhat in different ILs. Nonetheless, between the calculations and experimental spectra on other ILs, the assignments of the major spectral features are clear.

Consider the spectrum for neat [AMIM][DCA] (bottom, Figure 4). $[DCA]^-$ has no significant modes at frequencies above 2300 cm^{-1}, thus the poorly resolved structure between ∼2950 and 3150 cm^{-1} is assigned to the 11 CH stretch modes of $[AMIM]^+$, calculated to lie between 2945 and 3167 cm^{-1}. Conversely, there are no $[AMIM]^+$ modes calculated to lie between 2945 and 1641 cm^{-1}, thus the intense peaks at 2124 cm^{-1}, 2190 cm^{-1}, and 2226 cm^{-1} are assigned to symmetric and asymmetric C≡N stretches of $[DCA]^-$ and a combination band of the symmetric and asymmetric NC−N−CN stretches, consistent with literature assignments.[32,33] Mode 43 of $[AMIM]^+$ at 1641 cm^{-1} is the highest frequency skeletal mode, and has predominantly C=C stretch character. Given that there are no other $[AMIM]^+$ or $[DCA]^-$ modes with frequencies in the range between ∼1520−2900 cm^{-1}, we conclude that the C=C stretch must give rise to the small peak observed at 1647 cm^{-1}. This mode has low calculated IR intensity (0.8), thus its weakness is also consistent with the assignment. The bands at lower wavenumbers are difficult to assign unambiguously, but in the 1500−800 cm^{-1} range, they are mostly due to the ν_{27} $[AMIM]^+$ skeletal stretch or CH bending vibrations, none of which has significant C=C stretch character. $[DCA]^-$ has only one mode with high IR intensity in this range; the NC−N−CN asymmetric stretch, calculated to lie near ∼1323 cm^{-1}, presumably contributing to the strong peak at 1305 cm^{-1}, which probably also has some contribution from the $[AMIM]^+$ ν_{33} skeletal mode.

The spectrum for boron particles capped with [AMIM]-[DCA] has a strong band at ∼2480 cm^{-1} assigned to B_H stretching vibration of hydrogen atoms remaining on the surface (cf. Figure 2). Otherwise, comparison of the spectra for neat [AMIM][DCA] to that for the particles, shows that the C−H stretch vibrations are largely preserved in the [AMIM]-[DCA]-capped particles, as are many of the $[AMIM]^+$ skeletal vibrations. The weak C=C stretch mode, at 1647 cm^{-1} in the neat IL, is no longer apparent in the particle spectrum, although there is a weak new peak at 1701 cm^{-1}. The most obvious differences between the spectra are the substantial attenuations of the peaks associated with $[DCA]^-$ C≡N stretching (between 2124 and 2226 cm^{-1}), and of the strong peak at 1305 cm^{-1}, which also probably has a major contribution from the $[DCA]^-$ NC−N−CN asymmetric stretch. Definitive information about [AMIM][DCA] binding to boron would require unfeasibly difficult calculations of frequencies for an IL layer on a boron surface. The conclusion is that the vibrations associated with $[DCA]^-$ are far more strongly perturbed by binding to the surface than those associated with $[AMIM]^+$, suggesting that boron-$[DCA]^-$ interactions are important in the binding.

Figure 5 compares IR spectra for neat [MAT][DCA] and H_2-milled boron particles capped with [MAT][DCA]. As in Figure 4, there is a substantial B−H stretch band for the particle spectrum, and there is also substantial attenuation of the stretching modes of $[DCA]^-$ in the range between 2124 and 2226 cm^{-1}, suggesting that $[DCA]^-$ is involved in binding to boron. There is little change in the N−H and C−H stretching modes associated with the $[MAT]^+$ cation; however, there is stronger perturbation of the spectrum in the 600−1500 cm^{-1} range, corresponding to the $[MAT]^+$ skeletal vibrations, suggesting that $[MAT]^+$ is involved in bonding to boron. It is interesting to compare these spectra to those for [MAT]-[DCA]-capped particles prepared by milling directly in neat [MAT][DCA], without the intermediate H_2-milling step, i.e., for [MAT][DCA] interacting directly with boron, rather than a B−H-modified surface. In that spectrum, there was less loss of intensity associated with the C≡N stretching modes of $[DCA]^-$, however, there was substantial loss of intensity in the N−H stretching modes of the $[MAT]^+$ amine group, and in the 600−1500 cm^{-1} range where the $[MAT]^+$ skeletal modes lie.[20] The differences suggest that the mode of binding is affected by the presence of B−H bonds. In particular, $[DCA]^-$ appears to be more important in bonding to the B−H functionalized surface, while $[MAT]^+$ appears to be more important in binding to unfunctionalized boron.

Zeta potential measurements provide additional insight into the nature of the IL-surface bonding, by probing the net charge on the surface layer of the particles. Results are shown in Figure 6 for H_2-milled boron, mix milled with ILs, and dispersed in acetone. Acetonitrile/acetone was used as an inert, aprotic solvent to avoid any pH effects. For boron milled in acetonitrile (without H_2), and measured with no air exposure beyond that from O_2 diffusing into the acetonitrile, the zeta potential is essentially zero, indicating that the surface layer had approximately neutral polarity. If such particles are air-dried and resuspended, resulting in surface oxidation, the zeta potential becomes negative, possibly due to formation of surface hydroxyl groups from reaction with atmospheric water. For boron milled in H_2, and then capped with either

DOI: 10.1021/acsami.5b02366
ACS Appl. Mater. Interfaces 2015, 7, 9991−10003

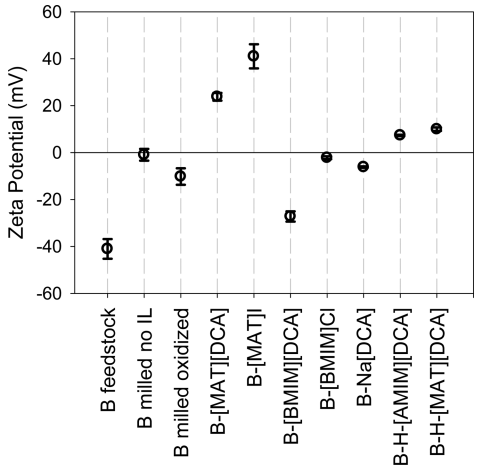

Figure 6. Zeta potential measurements for boron nanoparticles milled under different conditions. Data for IL capping of non-hydrogenated boron particles is taken from Perez et al.[20]

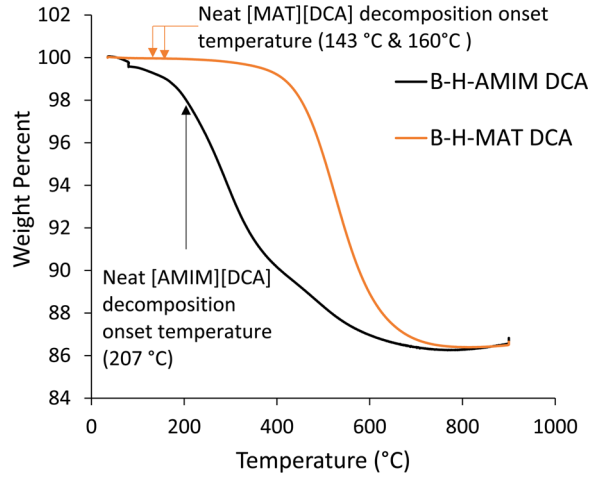

Figure 7. TGA analysis of boron particles produced by H_2 milling, followed by mix milling with the indicated ILs, and solvent washing to remove excess ILs.

[AMIM][DCA] or [MAT][DCA], the zeta potentials are slightly positive. For comparison, values are shown for boron particles produced by milled in neat [MAT][DCA] and [BMIM][DCA], with no intermediate H_2 milling step, and it can be seen that the zeta potentials are quite different. The strongly positive potential for B-[MAT][DCA], along with the IR spectrum for this sample, was taken as evidence that bonding of the IL to the surface was dominated by the $[MAT]^+$ cation, via its amine group.[20] For [BMIM][DCA], lacking the amine group, the strongly negative zeta potential was taken as evidence that bonding was primarily via the $[DCA]^-$ anion, consistent with the strong perturbations of the associated C≡N stretch modes in the particle IR spectrum. The small positive zeta potentials observed for hydrogenated boron subsequently capped with both [MAT][DCA] and [AMIM][DCA], as well as the strong perturbation of the $[DCA]^-$ vibrations (Figures 4 and 5), suggest that both the cation and anions are involved in interactions with the surface, such that the surface layer is left with a slight net positive charge.

To address the question of how much IL is bound to the particle surfaces in forming the solvent-resistant layer that protects the particles from air oxidation, we use thermogravimetric analysis. The two ILs used here both undergo decomposition to gaseous products under inert atmosphere, providing a simple way to estimate the IL coverage on as-prepared samples. Figure 7 shows thermal gravimetric analysis (TGA) of samples prepared by H_2-milling, following by mix-milling with either [AMIM][DCA] or [MAT][DCA], and then repeated ultrasonic washing with acetone to remove any weakly bound ligands. The TGA instrument is housed in a glovebox, and samples were transferred under nitrogen. In each experiment, the sample temperature was initially ramped to 80 °C, and then allowed to remain constant for 20 min to desorb acetone or other volatile species that might have remained from the solvent washing process. After this initial degassing period, the mass losses were measured as the temperature was ramped to 900 °C at a rate of 10 °C/min.

For comparison, the decomposition onset temperatures measured for the neat ILs are indicated in the figure as well. For [AMIM][DCA], the onset temperature of 207 °C is from Schneider et al.,[36] and that paper also reports an decomposition onset of 143 °C for [MAT][DCA]. In our previous study[20] of boron particles produced by milling directly in [MAT][DCA] (i.e., with no H_2 milling step), we reported TGA studies of both neat [MAT][DCA] and [MAT][DCA]-capped boron particles. For neat [MAT][DCA], initial decomposition began at ∼160 °C, with an abrupt increase in mass loss rate occurring at ∼190°. The somewhat higher initial decomposition temperature in this study may reflect improved purity of the later sample. For the [MAT][DCA]-capped boron particles produced without H_2 milling, a few percent of mass loss was observed below 190 °C, probably due to evaporation of the solvent used to wash the particles, and then the main mass loss (∼14%) occurred between ∼190 and 430 °C. The H_2-milled, [MAT][DCA]-capped particles in Figure 7 show similar percent mass loss, but only at substantially higher temperatures.

For the [AMIM][DCA]-capped sample, a small mass loss was observed during the degassing process, while the [MAT][DCA]-capped sample showed essentially no degassing. The [AMIM][DCA]-capped sample started to decompose at ∼100 °C, while the [MAT][DCA]-capped sample was stable up to ∼250 °C. Both samples exhibited a total mass loss of about 13% as the temperature was ramped to ∼700 °C, suggesting that the IL capping layer mass fraction was similar in both cases, which is perhaps not surprising given that [AMIM][DCA] and [MAT][DCA] have similar molecular weights and sizes. From the hydrogen loading of the particles, we estimate that the B−H-terminated surface area was ∼1200 m^2/g for uncapped, H_2-milled boron, although as noted, microscopy and DLS indicates that there is considerable aggregation of the particles, and it is likely that some of the B−H-capped surfaces are inaccessible to the IL during mix milling. If we assume that the ∼13% mass loss corresponds to complete loss of the IL capping ligands, and that the entire B−H-functionalized surface area was IL capped, then we can estimate that the initial IL capping layer density was ∼100 $\mu g/m^2$ corresponding to only ∼0.4 [AMIM][DCA] or [MAT][DCA] ion pairs per square nanometer of surface. This capping layer density would cover only about one-quarter of the surface, and would almost certainly be insufficient to passivate the particles against air oxidation.

This IL capping layer density can be compared to that estimated from similar TGA analysis of IL-capped boron particles prepared by milling boron feed stock directly in

DOI: 10.1021/acsami.5b02366
ACS Appl. Mater. Interfaces 2015, 7, 9991−10003

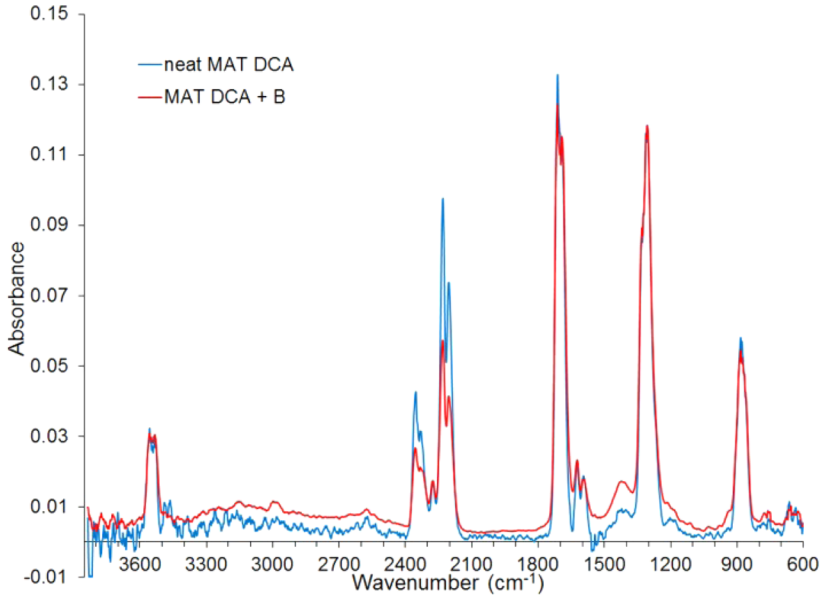

Figure 8. Infrared spectra of ignition of neat [MAT][DCA] (blue) and boron-infused [MAT][DCA] (red).

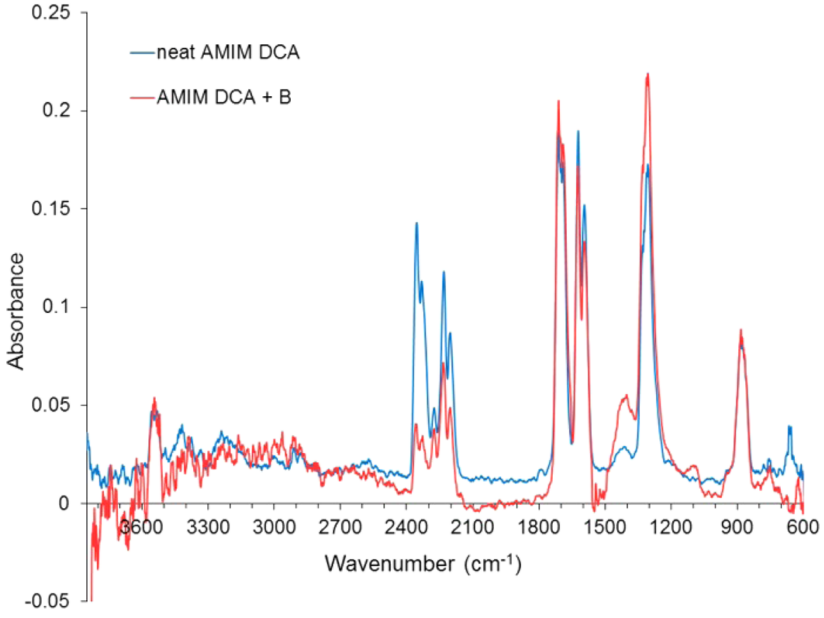

Figure 9. Infrared spectra of ignition of neat [AMIM][DCA] (blue) and boron-infused [AMIM][DCA] (red).

[MAT][DCA] and [BMIM][DCA] (i.e., without first milling in H_2).[20] In that paper, a number of approaches to interpreting the TGA data were examined, but for the assumption that the mass loss represented 100% ligand loss, the estimated IL capping layer densities were ~14 and ~1.8 ion pairs/nm^2 for [MAT][DCA] and [BMIM][DCA], respectively, the latter corresponding to about one close-packed monolayer on the surface. The actual percent mass losses in those experiments were no larger than those observed here for the H_2-milled, IL-capped particles. The factor responsible for the apparent large difference in estimated IL density is the assumed particle surface area. In the previous paper, the surface area (~40 m^2/g) was estimated from the particle size distribution obtained by DLS. For the H_2-milled particles, the 1200 m^2/g surface area was estimated from the hydrogen uptake, based on the theoretical result that the only stable binding site for hydrogen was on the surface, in the form of B−H bonds. SEM and STEM analysis of the H_2-milled particles,[20] and HeIM and DLS analysis of the IL-capped particles (Figure 1) suggest that the particles are actually aggregates formed by stacking of plate-like primary particles, and the high hydrogen loading implies that both the internal and external surfaces of the aggregates must be B−H-terminated. B−H capping of internal surfaces may result from H_2 diffusion into cracks between the primary particles, but it is also likely that a significant amount of aggregation takes place by cold welding of primary particle that were already B−H-terminated. It would not be surprising that such aggregates might have B−H-terminated cracks and internal voids that are inaccessible to the ion pairs comprising the viscous ILs, such that the effective IL-capped surface area is substantially smaller than 1200 m^2/g. Indeed, if we use the aggregated particle size (272 nm) determined by DLS to

DOI: 10.1021/acsami.5b02366
ACS Appl. Mater. Interfaces 2015, 7, 9991−10003

estimate the external surface area of equivalent spherical particles (~10 m^2/gram), then the estimated IL capping layer density would be ~48 ion pairs/nm^2. Given the highly convoluted structure of the aggregates (Figure 1), this is clearly an underestimate of the exposed surface area, and hence an overestimate of the IL density on the surface.

Effects of Particle Concentration on Ignition Delay. Several effects on hypergolic ignition and combustion of ILs might be expected from loading with boron nanoparticles. Because the initial reaction is between the oxidizer and IL, the particle mass may act as a heat sink, thereby retarding the rapid temperature needed for ignition. On the other hand, the particle surfaces may catalyze reactions, and radiative feedback from the reaction front to the particles may enhance heating of the reacting mixture. We previously reported hypergolic ignition measurements for several ILs containing boron nanoparticles at loadings of only ~0.33%, and found that the ignition delays were essentially unchanged from those for the neat ILs, as might be expected for such low loadings.[10,37] Combustion was more vigorous for the boron-loaded ILs, compared to the neat ILs, however, suggesting either that some boron combustion did occur, or that catalysis or radiative feedback from the flame front helped drive the reaction.

To have a significant effect on the energy density of IL propellants, boron loadings much greater than 0.3% would be required, and here we report the first hypergolic ignition experiments on ILs with boron loadings of up to ~25 wt %. As discussed above, the measurements were made by dropping white fuming nitric acid (WFNA) onto the surface of the IL, while monitoring the IR spectrum of vapors ~1 cm above the surface. Unfortunately, because of differences in the drop test methodology used here and in the previous studies, the absolute ignition delay times are not directly comparable.

Typical RS-FTIR spectra are shown in Figures 8 and 9 for [MAT][DCA] and [AMIM][DCA], with and without boron nanoparticles. As in hypergolic ignition RS-FTIR spectra obtained previously,[24] the peaks can be assigned as follows. HNO_3: 3550(m), 2995(w), 2586(w), 1710(s), 1300(s), 890(m), 758(w), 665(w) cm^{-1}; CO_2: 2350 cm^{-1}; HNCO: 2270 cm^{-1}; N_2O: 2220 cm^{-1}; and NO_2: 1610 cm^{-1}. Signals from these species dominate the spectra for ignition of the ILs with, and without, boron loading. Boron combustion might be expected to result in peaks (for the dominant ^{11}B isotopologs) for species such as BO (1862 cm^{-1}),[38] HOBO (3681, 2023, 904, 516 cm^{-1}), $B(OH)_3$ (3688.6, 1460, 1415, 1028, 992, 667 cm^{-1}),[39,40] and B_2O_3 (3241, 1542, 1184 cm^{-1}).[41] The only obvious new signals observed in the spectra taken after ignition of the boron-containing ILs are broad increases in intensity near 1420 and 1100 cm^{-1}. The absence of other peaks associated with likely boron-containing products suggests that these apparent signals may simply be artifacts of baseline shifts because of signal averaging. It is, perhaps, unsurprising that boron-containing products are insignificant in the gas phase under these conditions, as such species have low vapor pressures at the temperatures in the RS-FTIR detection volume.

Figure 10 shows typical data for the 2350 cm^{-1} peak from CO_2 as a function of time, during the ignition process, for both neat [MAT][DCA] and [MAT][DCA] loaded with 25 wt % boron nanoparticles. Figure 11 summarizes the trend of ignition delay vs boron nanoparticle loading for both [MAT][DCA] and [AMIM][DCA]. The estimated ±0.3 s. uncertainty from the measurement method is indicated by error bars plotted on

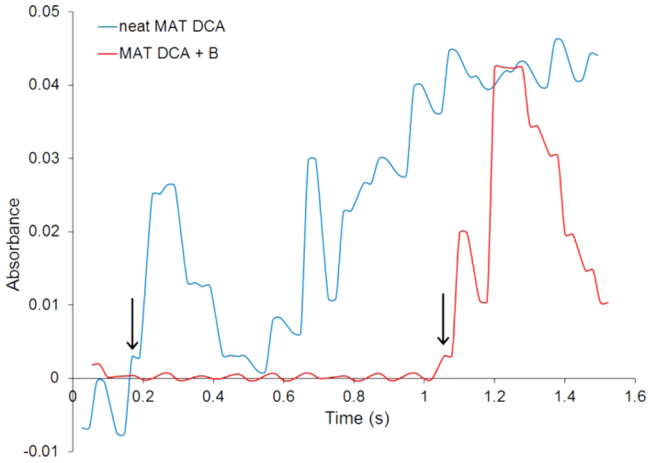

Figure 10. Determination of ignition delay time from monitoring CO_2 production at 2350 cm^{-1} during the drop tests. The arrows indicate the ignition delay times for neat [MAT][DCA] and [MAT][DCA] with 25 wt % B nanoparticles.

the [AMIM][DCA] data points. In spite of the relatively large timing uncertainties, a trend toward longer ignition delay times with increasing boron loading is apparent, as might be expected from the heat sink capacity of the boron, which should tend to slow the temperature rise leading to ignition. The ignition delay time for [MAT][DCA] increases from ~150 ms for the neat IL, to ~1 s for ~25 wt % boron loading. Interestingly, the effect of boron loading on ignition of [AMIM][DCA] is much weaker. Indeed, the increase (from ~100 ms for neat [AMIM][DCA] to ~400 ms for 27 wt % loading) is just at the uncertainly limit of the method.

It has been previously proposed that reaction of WFNA with the [DCA] anion is the main driver of hypergolic ignition for [DCA]-based salts, and that the contribution of the cation to the ignition behavior for these ILs is minimal.[24] The observation that neat [MAT][DCA] and [AMIM][DCA] have similar ignition delay times is consistent with this idea. One might expect that the ignition delay sensitivity to particle loading might be correlated to the thermal decomposition temperature of the IL, and in particular to the generation of gaseous decomposition products, because hypergolic ignition occurs in the gas phase.[24] The thermal decomposition onset temperatures for neat [MAT][DCA] and [AMIM][DCA], as measured by TGA, are 143 and 207 °C,[36] respectively. We might, therefore, expect that the less thermally stable IL ([MAT][DCA]) should generate gas and ignite more rapidly, and thus be less sensitive to the boron loading than [AMIM][DCA], contrary to the observed behavior. There are, however, several other factors to consider.

One factor that may lead to cation-specific differences in the sensitivity of the ignition delay time to boron nanoparticle loading is the viscosity of the IL: [AMIM][DCA] η = 42 cP and [MAT][DCA] η = 92 cP.[36] At high particle loadings, mixing and diffusion of WFNA into the IL is retarded not only by the viscosity of the IL, but also by the excluded volume taken up by the boron nanoparticles, which the WFNA cannot diffuse through. If the IL viscosity is high, the excluded volume effect may become more important, hence the larger particle effect on ignition of [MAT][DCA]

In addition, there may be inherent effects of boron surface chemistry on the ignition process. There is simply not enough information to speculate intelligently about possible catalytic

DOI: 10.1021/acsami.5b02366
ACS Appl. Mater. Interfaces 2015, 7, 9991−10003

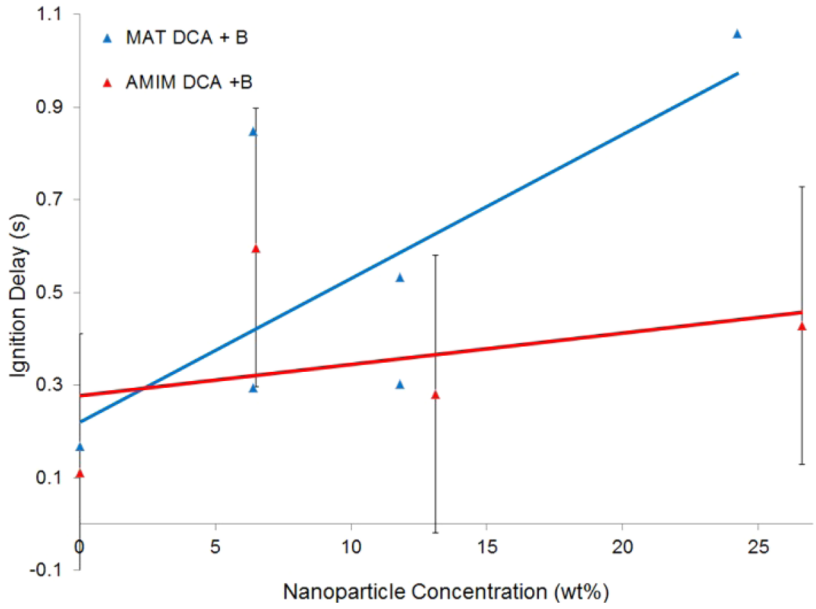

Figure 11. Dependence of hypergolic ignition delay time as a function of boron nanoparticle weight percent in [MAT][DCA] (blue) and [AMIM][DCA] (red). The uncertainty estimate for the ignition delay times is ±0.3 s (shown only on [AMIM][DCA] in the graph for clarity).

effects of the boron surfaces, however, Figure 7 shows a different effect of the IL-boron particle interaction. Note that [MAT][DCA]-capped particles begin to lose mass rapidly only above ~400 °C, compared to 143 °C for neat [MAT][DCA]. This temperature difference indicates that interaction of [MAT][DCA] with the boron particles produces a capping layer that is much more thermally stable than the neat IL. In contrast, [AMIM][DCA]-capped boron begins to lose mass near 200 °C, i.e., at nearly the same temperature as neat [AMIM][DCA], indicating that its thermal stability is not significantly affected by binding to boron. The highly stable [MAT][DCA] capping layer could have at least two effects. First, the presence of a stable capping layer represents additional unreactive mass in the boron-loaded [MAT][DCA] suspensions, and the added heat capacity would tend to further retard heating and ignition. In addition, we expect that as the IL capping layer is degraded, reaction of the initially unoxidized boron surfaces with WFNA should result in significant heat release, increasing with the boron loading. For [AMIM][DCA]-capped boron, this additional heating process should begin at low temperatures, compensating for the extra heat capacity of the boron, and moderating the increase in ignition delay time with particle loading. The highly stable capping layer formed by [MAT][DCA] would tend to inhibit this compensating heat release, resulting in a strong growth in ignition delay time with particle loading.

Although the RS-FTIR method used here did not allow observation of flame properties, the relatively weak dependence of ignition delay on loading is encouraging from the perspective of increasing energy density. If boron combustion were efficient, the volumetric enthalpy of combustion would be nearly doubled by addition of 27 wt % of boron, from ~35 to ~63 kJ/mL.

CONCLUSION

Milling of boron in H_2, followed by mix-milling with a capping agent, is shown to be an efficient way to produce boron nanoparticles capped with either alkyl groups or ionic liquids. IR spectroscopy suggests that the alkyl capping process involves reaction of terminal C═C bonds in alkene capping agents with B−H bonds on the surface, resulting in B−C bond formation. For the ionic liquids, the mode of binding to the surface is more difficult to determine unambiguously. There is no obvious difference in the mode of binding of ILs with and without terminal C═C bonds ([AMIM][DCA] and [MAT][DCA], respectively), and the strong perturbation of the C≡N stretching vibrations of the $[DCA]^-$ anion in the capping layer suggests that boron-[DCA] interaction is important in the bonding. Both IR and zeta potential measurements suggest that for [MAT][DCA]-capped particles, the mode of binding is somewhat different for particles with, and without hydrogen termination.

Both alkyl- and IL-capped particles are protected against air oxidation, even if the samples are repeatedly ultrasonicated in solvents to remove any weakly complexed capping agents. Several mechanisms may contribute to the oxidation resistance. The organic capping layers may physically exclude O_2 and water (the primary atmospheric oxidants) to some extent, however, given that the samples were heated overnight to 350 K, (octene boiling point = 394 K), and exposed to air for at least 6 h prior to XPS analysis, it seems unlikely the capping layer could simply be functioning as a diffusion barrier. More likely, bonding of the capping layer to the surface changes the surface chemistry, such that it is unreactive to O_2 and water up to 350 K.

AUTHOR INFORMATION

Corresponding Author

*E-mail: anderson@chem.utah.edu.

Author Contributions

The manuscript was written through contributions of all authors. All authors have given approval to the final version of the manuscript.

Funding

AFOSR grants FA9550-08-1-0400, FA9550-12-1-0481, FA9300-06-C-0023.

DOI: 10.1021/acsami.5b02366
ACS Appl. Mater. Interfaces 2015, 7, 9991−10003

Notes

The authors declare no competing financial interest.

■ ACKNOWLEDGMENTS

The Utah authors acknowledge support from the Air Force Office of Scientific Research under AFOSR MURI Grant FA9550-08-1-0400 and BRI Grant FA9550-12-1-0481. This work made use of University of Utah shared facilities of the Micron Technology Foundation Inc. Microscopy Suite sponsored by the College of Engineering, Health Sciences Center, Office of the Vice President for Research, and the Utah Science Technology and Research (USTAR) initiative of the State of Utah. Helium ion microscopy was done by Dr. Doug Wei, of the Carl Zeiss Microscopy Ion Microscopy Innovation Center. The hypergolic ignition studies were supported by grant FA9300-06-C-0023 from AFOSR. [MAT][DCA] was synthesized by Dr. Stefan Schneider at the Air Force Research Lab/Edwards AFB, also with support from AFOSR grant FA9300-06-C-0023.

■ REFERENCES

(1) Cox, J. D.; Wagman, D. D.; Medvedev, V. A. *Codata Key Values for Thermodynamics*. Hemisphere Publishing: Carlsbad, CA, 1989.
(2) Hsia, H. T.-S. *Air-Augmented Combustion of Boron and Boron-Metal Alloys*; Air Force Rocket Propulsion Laboratory, Air Force Systems Command, United States Air Force: Edwards, CA, 1971.
(3) Jain, A.; Anthonysamy, S.; Ananthasivan, K.; Gupta, G. S. Studies on the Ignition Behaviour of Boron Powder. *Thermochim. Acta* **2010**, *500*, 63−68.
(4) Jain, A.; Joseph, K.; Anthonysamy, S.; Gupta, G. S. Kinetics of Oxidation of Boron Powder. *Thermochim. Acta* **2011**, *514*, 67−73.
(5) Kuo, K. K.; Risha, G. A.; Evans, B. J.; Boyer, E. Potential Usage of Energetic Nano-Sized Powders for Combustion and Rocket Propulsion. *Mater. Res. Soc. Symp. Proc.* **2004**, *800*, 3−14.
(6) Mitani, T.; Izumikawa, M. Combustion Efficiencies of Aluminum and Boron Propellants. *J. Spacecraft Rockets* **1991**, *28*, 78−84.
(7) Risha, G. A.; Boyer, E.; Evans, B.; Kuo, K. K.; Malek, R. Characterization of Nano-Sized Particles for Propulsion Applications. *Mater. Res. Soc. Symp. Proc.* **2003**, *800*, 243−254.
(8) Young, E. A.; Yang, Y. Preparation and Properties of $Mg(B_{1-x}C_x)_2$ Using Carbon Chemical Vapor Coated Boron. *IEEE Trans. Appl. Supercond.* **2007**, *17*, 2794−2797.
(9) Hsieh, W.-H.; Peretz, A.; Huang, I.-T.; Kuo, K. K. Combustion Behavior of Born-Based Bamo/Nmmo Fuel-Rich Solid Propellants. *J. Propulsion* **1991**, *7*, 497−503.
(10) Perez, J. P. L.; McMahon, B. W.; Yu, J.; Schneider, S.; Boatz, J. A.; Hawkins, T. W.; McCrary, P. D.; Flores, L. A.; Rogers, R. D.; Anderson, S. L. Boron Nanoparticles with High Hydrogen Loading: Mechanism for B−H Binding and Potential for Improved Combustibility and Specific Impulse. *ACS Appl. Mater. Interfaces* **2014**, *6*, 8513−8525.
(11) Linstrom, P. J.; Mallard, W. G. *NIST Chemistry Webbook, NIST Standard Reference Database Number 69*; National Institute of Standards and Technology: Gaithersburg, MD, 2011; p 20899.
(12) Devaprabhakara, D.; Sethi, D. S. Recent Progress in the Hydroboration Reactions. *J. Sci. Ind. Res.* **1970**, *29*, 280−292.
(13) Beckett, M. A. Boron. *Annu. Rep. Prog. Chem. Sect. A: Inorg. Chem.* **1994**, *90*, 3−24.
(14) Fu, G. C. Metal-Catalyzed Hydroboration Reactions. *Trans. Met. Org. Synth.* **1998**, *2*, 141−146.
(15) Renaud, P.; Beauseigneur, A.; Brecht-Forster, A.; Becattini, B.; Darmency, V.; Kandhasamy, S.; Montermini, F.; Ollivier, C.; Panchaud, P.; Pozzi, D.; Scanlan, E. M.; Schaffner, A.-P.; Weber, V. Boron: A Key Element in Radical Reactions. *Pure Appl. Chem.* **2007**, *79*, 223−233.
(16) Zhang, Q.; Shreeve, J. n. M. Energetic Ionic Liquids as Explosives and Propellant Fuels: A New Journey of Ionic Liquid Chemistry. *Chem. Rev.* **2014**, *114*, 10527−10574.
(17) Van Devener, B.; Perez, J. P. L.; Anderson, S. L. Air-Stable, Unoxidized, Fuel-Soluble Boron Nanoparticles. *J. Mater. Res.* **2009**, *24*, 3462−3464.
(18) Van Devener, B.; Perez, J. P. L.; Jankovich, J.; Anderson, S. L. Oxide-Free, Catalyst-Coated, Fuel-Soluble, Air-Stable Boron Nanopowder as Combined Combustion Catalyst and High Energy Density Fuel. *Energy Fuels* **2009**, *23*, 6111−6120.
(19) Perez, J. P. L.; McMahon, B. W.; Anderson, S. L. Functionalization and Passivation of Boron Nanoparticles with a Hypergolic Ionic Liquid. *J. Propul. Power* **2013**, *29*, 489−495.
(20) Perez, J. P. L.; McMahon, B. W.; Schneider, S.; Boatz, J. A.; Hawkins, T. W.; McCrary, P. D.; Beasley, P. A.; Kelley, S. P.; Rogers, R. D.; Anderson, S. L. Exploring the Structure of Nitrogen-Rich Ionic Liquids and Their Binding to the Surface of Oxide-Free Boron Nanoparticles. *J. Phys. Chem. C* **2013**, *117*, 5693−5707.
(21) Gao, Z.; Walton, N. I.; Malugin, A.; Ghandehari, H.; Zharov, I. Preparation of Dopamine-Modified Boron Nanoparticles. *J. Mater. Chem.* **2012**, *22*, 877.
(22) McMahon, B. W.; Perez, J. P. L.; Yu, J.; Boatz, J. A.; Anderson, S. L. Synthesis of Nanoparticles from Malleable and Ductile Metals Using Powder-Free, Reactant-Assisted Mechanical Attrition. *ACS Appl. Mater. Interfaces* **2014**, *6*, 19579−19591.
(23) Hawkins, T. W.; Schneider, S.; Drake, G. W.; Vaghjiani, G.; Chambreau, S. Hypergolic Fuels. U.S. Patent 8 034 202, Oct 11, 2011.
(24) Chambreau, S. D.; Schneider, S.; Rosander, M.; Hawkins, T.; Gallegos, C. J.; Pastewait, M. F.; Vaghjiani, G. L. Fourier Transform Infrared Studies in Hypergolic Ignition of Ionic Liquids. *J. Phys. Chem. A* **2008**, *112*, 7816−7824.
(25) Sharma, B. K. *Instrumental Methods of Chemical Analysis*; Krishna Prakashan: Uttar Pradesh, India, 2000.
(26) Yang, T.; Berber, S.; Liu, J.-F.; Miller, G. P.; Tománek, D. Self-Assembly of Long Chain Alkanes and Their Derivatives on Graphite. *J. Chem. Phys.* **2008**, *128*, 124709/1−124709/8.
(27) Shirley, D. A. High-Resolution X-Ray Photoemission Spectrum of the Valence Bands of Gold. *PHys. Rev. B* **1972**, *5*, 4709−4714.
(28) Moulder, J. F.; Stickle, W. F.; Sobol, P. E.; Bomben, K. D. *Handbook of X-Ray Photoelectron Spectroscopy*; Chastain, J., King, R. C., Jr., Eds.; Physical Electronics: Eden Prarie, MN, 1995.
(29) Nohira, H.; Hattori, T. Oxidation of H-Terminated Silicon. *Springer Ser. Mater. Sci.* **2001**, *46*, 61−88.
(30) Niwano, M.; Kageyama, J.-i.; Kinashi, K.; Sawahata, J.-i.; Miyamoto, N. Oxidation of Hydrogen-Terminated Si Surfaces Studied by Infrared Spectroscopy. *Surf. Sci.* **1994**, *301*, L245−L249.
(31) Wagner, C. D.; Naumkin, A. V.; Kraut-Vass, A.; Allison, J. W.; Powell, C. J.; Jr., J. R R. Nist X-Ray Photoelectron Spectroscopy Database. http://srdata.nist.gov/xps/.
(32) Lotsch, B. V.; Senker, J.; Kockelmann, W.; Schnick, W. Investigation of Structural and Dynamic Properties of $Nh_4[N(CN)_2]$ by Means of X-Ray and Neutron Powder Diffraction as Well as Vibrational and Solid-State Nmr Spectroscopy. *J. Solid State Chem.* **2003**, *176*, 180−191.
(33) Jürgens, B.; Höppe, H. A.; Shchnick, W. Synthesis, Crystal Structure, Vibrational Spectroscopy, and Thermal Behaviour of Lead Dicyanamide $Pb[N(CN)_2]_2$. *Solid State Sci.* **2002**, *4*, 821−825.
(34) Frisch, M. J.; Trucks, G. W.; Schlegel, H. B.; Scuseria, G. E.; Robb, M. A.; Cheeseman, J. R.; Scalmani, G.; Barone, V.; Mennucci, B.; Petersson, G. A.; Nakatsuji, H.; Caricato, M.; Li, X.; Hratchian, H. P.; Izmaylov, A. F.; Bloino, J.; Zheng, G.; Sonnenberg, J. L.; Hada, M.; Ehara, M.; Toyota, K.; Fukuda, R.; Hasegawa, J.; Ishida, M.; Nakajima, T.; Honda, Y.; Kitao, O.; Nakai, H.; Vreven, T.; Montgomery Jr., J. A.; Peralta, J. E.; Ogliaro, F.; Bearpark, M. J.; Heyd, J.; Brothers, E. N.; Kudin, K. N.; Staroverov, V. N.; Kobayashi, R.; Normand, J.; Raghavachari, K.; Rendell, A. P.; Burant, J. C.; Iyengar, S. S.; Tomasi, J.; Cossi, M.; Rega, N.; Millam, N. J.; Klene, M.; Knox, J. E.; Cross, J. B.; Bakken, V.; Adamo, C.; Jaramillo, J.; Gomperts, R.; Stratmann, R. E.; Yazyev, O.; Austin, A. J.; Cammi, R.; Pomelli, C.;

DOI: 10.1021/acsami.5b02366
ACS Appl. Mater. Interfaces 2015, 7, 9991−10003

Ochterski, J. W.; Martin, R. L.; Morokuma, K.; Zakrzewski, V. G.; Voth, G. A.; Salvador, P.; Dannenberg, J. J.; Dapprich, S.; Daniels, A. D.; Farkas, Ö.; Foresman, J. B.; Ortiz, J. V.; Cioslowski, J.; Fox, D. J. *Gaussian 09*, Gaussian, Inc.: Wallingford, CT, 2009.

(35) Scott, A. P.; Radom, L. Harmonic Vibrational Frequencies: An Evaluation of Hartree-Fock, Møller-Plesset, Quadratic Configuration Interaction, Density Functional Theory, and Semiempirical Scale Factors. *J. Phys. Chem.* **1996**, *100*, 16502−16513.

(36) Schneider, S.; Hawkins, T.; Rosander, M.; Vaghjiani, G.; Chambreau, S.; Drake, G. Ionic Liquids as Hypergolic Fuels. *Energy Fuels* **2008**, *22*, 2871−2872.

(37) McCrary, P. D.; Beasley, P. A.; Cojocaru, O. A.; Schneider, S.; Hawkins, T. W.; Perez, J. P.; McMahon, B. W.; Pfeil, M.; Boatz, J. A.; Anderson, S. L.; Son, S. F.; Rogers, R. D. Hypergolic Ionic Liquids to Mill, Suspend, and Ignite Boron Nanoparticles. *Chem. Commun.* **2012**, *48*, 4311−4313.

(38) Huber, K. P.; Herzberg, G. *Molecular Spectra and Molecular Structure IV. Constants of Diatomic Molecules*; Van Nostrand Reinhold: New York, 1979;.

(39) Andrews, L.; Burkholder, T. R. Infrared Spectra of Molecular $B(Oh)_3$ and HOBO in Solid Argon. *J. Chem. Phys.* **1992**, *97*, 7203−7210.

(40) Gilson, T. R. Characterisation of Ortho- and Meta-Boric Acids in the Vapour Phase. *J. Chem. Soc., Dalton Trans.* **1991**, 2463−2466.

(41) Ramos, A. S.; Taguchi, S. P.; Ramos, E. C. T.; Arantes, V. L.; Ribeiro, S. High-Energy Ball Milling of Powder B-C Mixtures. *Mater. Sci. Eng., A* **2006**, *A422* (1−2), 184−188.

DOI: 10.1021/acsami.5b02366
ACS Appl. Mater. Interfaces 2015, 7, 9991−10003